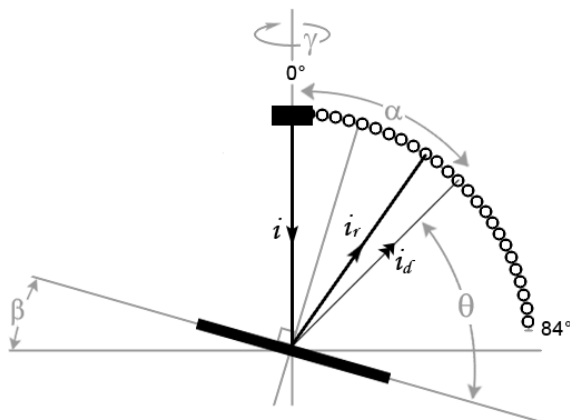


**Electronic supplementary information.**



**Figure ESI-1.** Scheme of the goniometric set up.

**Table ESI-2.** Conditions of 1  $\mu\text{m}$  colloidal silica synthesis by Stöber and Nozawa processes.

Series	Reaction medium	V <sub>total</sub> (mL)	Constant adding reactant	V <sub>total</sub> (mL)	Addition rate (mL.h <sup>-1</sup> )	Silica size ( $\mu\text{m}$ )
	[TEOS] / [NH <sub>4</sub> OH] / [EtOH]	122	0.9 / 14	50	4	1

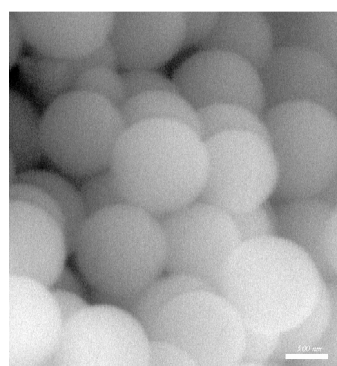


**Figure ESI-3.** ESEM Images of 1 mm monodisperse colloidal silica particles synthesized by following Table 1 parameters (Scale bar: 500nm).

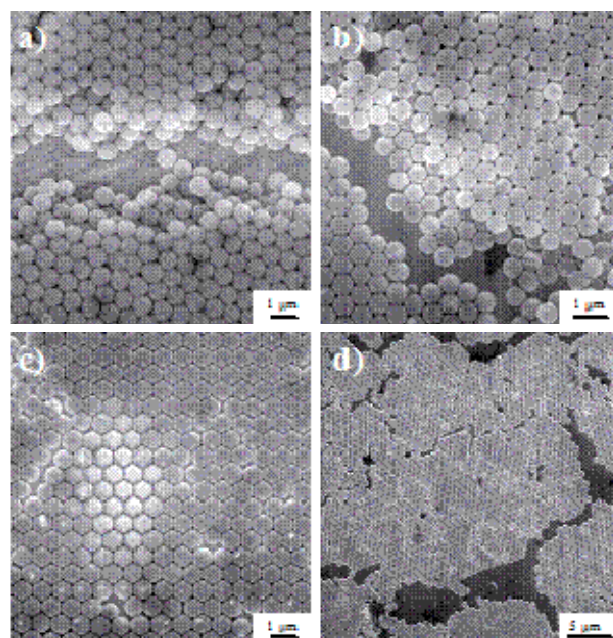


**Figure ESI-4.** ESEM observations after dip-coating deposition for a 15 vol.% solution of hybrid silica particles with various withdrawal rate (a) 3 layers at  $4 \text{ mm.s}^{-1}$  (entry A1), (b) 2 layers at  $3 \text{ mm.s}^{-1}$  (entry A2), (c) 1 layer at  $1 \text{ mm.s}^{-1}$  (entry A3) and (d) hole apparition at  $0.5 \text{ mm.s}^{-1}$  (entry A4).

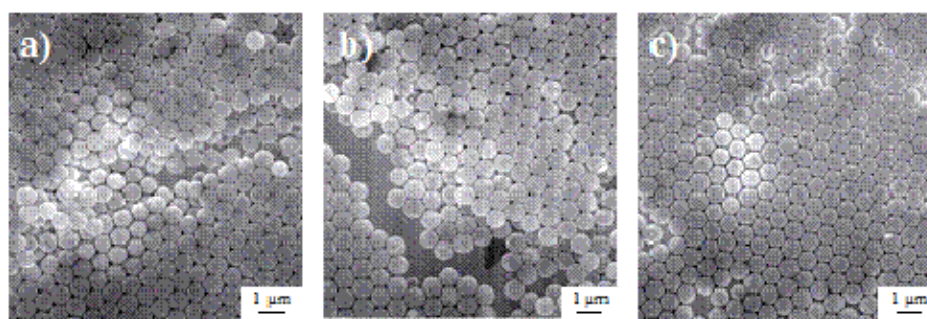


**Figure ESI-5.** ESEM observations for  $3 \text{ mm.s}^{-1}$  withdrawal rate for various volume fraction of core@shell silica particles a) 3 layers with 25 vol.% (entry B1) b) 2 layers with 15 vol.% (entry A2) and c) 1 layer with 3 vol.% (entry C1).

**Table ESI-6.** Determination of the silica particles diameter  $\Phi$  from Figure 8 according eq. 5 with  $d_1 = \frac{\sqrt{3}}{2}\Phi$  for a hexagonal array and  $d_2 = \Phi$  for a cubic one.

Angle (°)	$\Phi$ (nm)		
	Order 1 hexagonal	Order 2' cubic	Order 2 hexagonal
30	1016		
33	1011		
36	1022		
39	1024		
42	1032		
45	1028		
48	1038		
54		1016	
57		1016	
60		1037	
63		1030	
66		1039	1036
69		1030	1037
72		1025	1026
75		1037	1030
78		1033	1031
Average (nm)	1029	1029	1032
Deviation (nm)	5.9	3.5	2.3

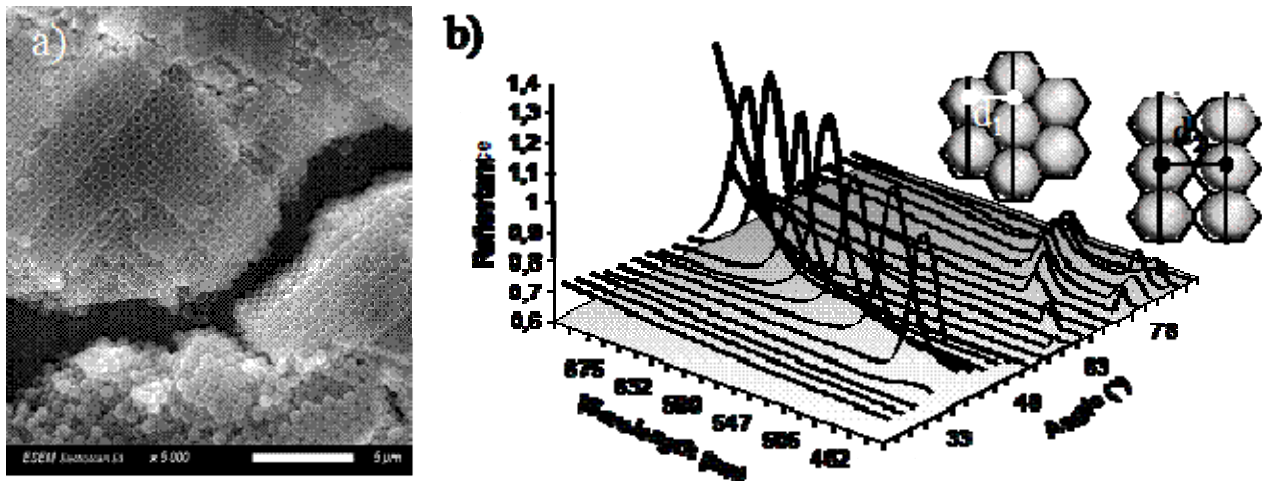


**Figure ESI-7A.** a) ESEM observation of a colloidal crystal composed of 8 layers with cubic phase and b) diffraction at normal incidence of  $1\mu\text{m}$  core@shell particles network in hexagonal and cubic arrays (first and second order) (Table ESI-6 in electronic supporting information).

Indeed, for 3 to 8 coated layers, no real evolution of the diffraction figure was observed. The number of layers is considered as being too low to generate analyzable constructive 3D interferences. The validity of a 2D explanation is confirmed by the constant character of  $d$  for all the observable diffraction order. In addition, its value match at 96% with those deducted from ESEM analyses. The ESEM value of  $d$  was related to the diameter and the crystallographic structure, for example  $d_1 = \frac{\sqrt{3}}{2}\Phi$  for a hexagonal array and  $d_2 = \Phi$  for a cubic one.

The good correlation found for  $d$  values indicate a 3D structure related to a hexagonal compact (*hcp*). Up to now, due to the similarity between the 2D space of a *hcp* (001) and the *fcc* (111) plans, we were not able to assume one 3D structure more than the other one.

Depending on the self-assembly,  $d$  can also be related to the structure modification as a cubic or a hexagonal array. Indeed, as showed in some colloidal crystals, defaults are created. As demonstrated in Figure 8, defaults are able to propagate until new structures were locally generated. So, according to the diffracted wavelength, the nature of the structure and its order can be determined.

The goniometric technique is enough sensitive to discriminate the various structures on the diffraction pattern. The main diffraction peaks is always due to the *hcp* array, but the diffraction pattern can also show two new bands which following the increasing angle and are attributed to the cubic then to the hexagonal second order of diffraction in accordance with the *d* calculation checking (Figure ESI-7A and Table ESI-6).

In addition, In order to obtain a larger pattern of diffraction, the angle of incidence has been modified by a substrate tilt by rotation of an angle  $\beta$  (Figure ESI-1 and ESI-7B).

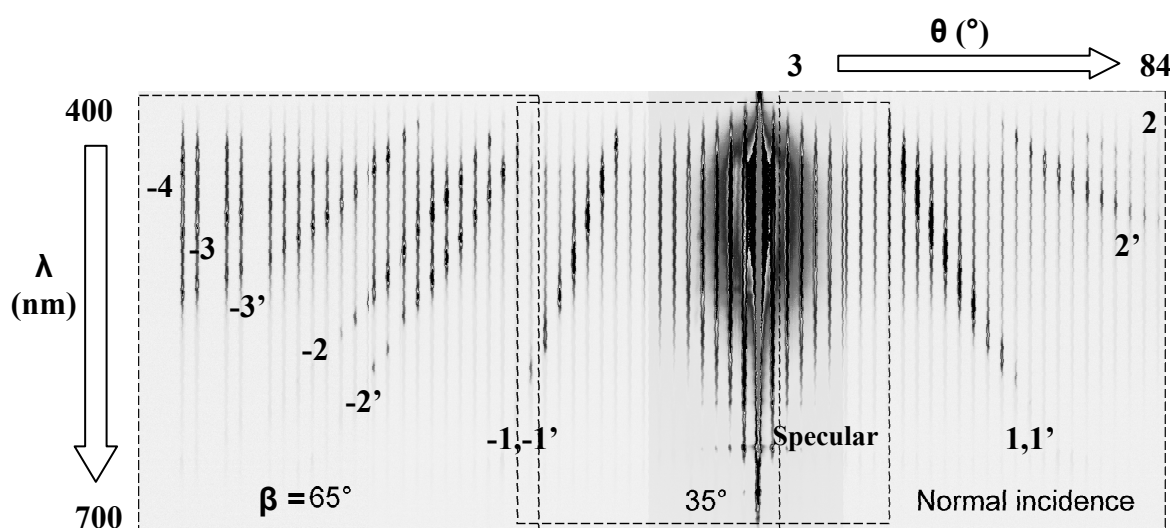


**Figure ESI-7B.** Reconstitution of the diffracted pattern of  $1\text{ }\mu\text{m}$  core@shell particles grating at different incident angle (from  $\beta = 0^\circ$  to  $65^\circ$ ). Classic number identifies hexagonal order and the prime the cubic order.

In Figure ESI-7B, a reconstruction of the diffraction pattern at various angles of incidence can be represented. Each vertical line represents an optic fiber whose level is proportional to the 400-700nm wavelength range. These points of observation are separated each other from 3 degrees. The black peak corresponds to a diffracted wavelength and their linear alignments to an order of diffraction. The large central black band corresponds to the reflected beam ( $I_r$ ) or so- called ‘specular’ beam (Figure ESI-7B).

At normal incidence, we conserve the diffraction pattern presented in Figure 8, *i.e.* two hexagonal and cubic structures, mixed for the 1<sup>st</sup> order and deconvoluted for the 2<sup>nd</sup> one. When the angle increases up to 35°, the specular beam and then the emergence of the hexagonal negative first order appear. The higher orders appear at 65° by presenting an (- 4) and reasonably (- 3) diffraction orders, for hexagonal and cubic structures, respectively. The progressive increasing gap between the lines along the various orders confirmed the double nature of the structure. Equivalent experiences in transmission were carried out. The first results show similar diffraction behaviours in term of wavelengths and angles values which traduces planar diffraction symmetry of the sample. Here, a rapid dip-coating process allows the elaboration of colloidal crystal structures which exhibit angle-dependent photonic properties.